Nuclear Instruments and Methods in Physics Research A 610 (2009) 1–10

Contents lists available at ScienceDirect

Nuclear Instruments and Methods in Physics Research A

journal homepage: www.elsevier.com/locate/nima

Nanotechnology: A new era for photodetection?

M. Ambrosio [a,*], A. Ambrosio [a,b], G. Ambrosone [a,b], L. Campajola [a,b], G. Cantele [a,b], V. Carillo [a,b], U. Coscia [a,b], G. Iadonisi [a,b], D. Ninno [a,b], P. Maddalena [a,b], E. Perillo [a,b], A. Raulo [a,b], P. Russo [a,b], F. Trani [a,b], E. Esposito [a,c], V. Grossi [a,d], M. Passacantando [a,d], S. Santucci [a,d], M. Allegrini [a,e], P.G. Gucciardi [a,f], S. Patanè [a,g], F. Bobba [a,h], A. Di Bartolomeo [a,h], F. Giubileo [a,h], L. Iemmo [a,h], A. Scarfato [a,h], A.M. Cucolo [a,h]

[a] INFN Sezione di Napoli, Via Cintia 2, 80125 Napoli, Italy
[b] Dipartimento di Fisica, Università "Federico II" di Napoli, Italy
[c] Istituto di Cibernetica "E. Caianiello", Italy
[d] Dipartimento di Fisica, Università dell'Aquila, Italy
[e] Dipartimento di Fisica, Universià di Pisa, Italy
[f] CNR—IPCF Sezione di Messina, Italy
[g] Dipartimento di Fisica della Materia and TFA, Università di Messina, Italy
[h] Dipartimento di Fisica, Università di Salerno, Italy

ARTICLE INFO

Available online 29 May 2009

Keywords:
Carbon nanotube
Photodetector
Field emission

ABSTRACT

Nowadays we live in the so-called "Silicon Era", in which devices based on the silicon technology permeate all aspects of our daily life. One can simply think how much silicon is in the everyday household objects, gadgets and appliances.

The impact of silicon technology has been very relevant in photodetection as well. It enables designing large or very large-scale integration devices, in particular microchips and pixelled detectors like the Silicon Photo Multiplier made of micrometric channels grouped in mm^2 pixels. However, on the horizon, the recent development of nanotechnologies is opening a new direction in the design of sub-micron photodevices, owing to the capability to deal with individual molecules of compounds or to chemically grow various kinds of materials.

Among them, carbon compounds appear to be the most promising materials being chemically very similar to silicon, abundant and easy to handle. In particular, carbon nanotubes (CNT) are a very intriguing new form of material, whose properties are being studied worldwide providing important results.

The photoelectric effects observed on carbon nanotubes indicate the possibility to build photodetectors based on CNTs inducing many people to claim that we are at the beginning of a Post Silicon Era or of the Carbon Era.

In this paper, we report on the most important achievements obtained on the application of nanotechnologies to photodetection and medical imaging, as well as to the development of radiation detectors for astro-particle physics experiments.

1. Introduction

The birth of Silicon Era usually is referred to the year 1958, when Jack Kilby, Nobel Price 2000, created the first integrated circuit at Texas Instruments to prove that resistors and capacitors could exist on the same piece of semiconductor material. His circuit consisted of a sliver of germanium with five components linked by wires. This has been the first integrated circuit whose backbone was the silicon wafer in which the circuit was directly carved. This approach opened the way to make more powerful, smaller and cheaper electronics devices. Starting from this achievement, the modern world has been fully based on silicon technology, by which every aspect of our life is imbibed: internet, computers, television, integrated circuits, but also pace-makers, solar energy, artificial prothesis, digital camera, GPS navigator, etc. Starting from raw silicon, we can produce silicon wafers, apply lithographed masks, carve inside and obtain electronic chips for our electronic devices with lower and lower costs and higher capabilities. To date, microelectronics has developed according to Moore's law stating that every two years the number of transistor in a chip doubles while the cost halves.

From the point of view of photodetection, the most advanced by-product of silicon technology is the silicon photomultiplier (SiPM), a single photon detector made of silicon pixels, as small as

* Corresponding author.
E-mail address: ambrosio@na.infn.it (M. Ambrosio).

0168-9002/$ - see front matter © 2009 Elsevier B.V. All rights reserved.
doi:10.1016/j.nima.2009.05.138

$40\,\mu m^2$, grouped in arrays a few square centimetres wide [1]. SiPM is able to detect individual photons and multiply the corresponding photoelectron through the silicon substrate up to a factor 10^5, producing in this way a detectable signal. SiPMs need still additional developments: they present great thermal noise and low efficiency in the UV wavelength region, but they are available on the market, and thus are relatively cheap and ready to be intensively used for applications. In the medical diagnostics, one of the best achievement is MEDIPIX 2, the chip that allows X-ray detection of organic materials with a pitch of 55 μm. In a $1.4 \times 1.6\,cm^2$ area, 256×256 readout channels are allocated.

In April 2007, Intel presented the Xeon Family Processor (PENRYN) based on transistor with 45 nm gate. With roughly twice the density of Intel® 65 nm technology, Intel's 45 nm contains about twice the number of transistors into the same silicon space, i.e. more than 400 million transistors for dual-core processors and more than 800 million for quad-core ones.

So far Gordon Moore's law is still appliable; however, physical limits appear at the horizon. First of all, the silicon semiconductor cannot efficiently transport current in thinner matter layers owing to quantum effects, which become non-negligible; moreover joule effect in the electron transport produces a high amount of heat to be dispersed. As thinner is the material layer as difficult is to avoid damages produced by heat production in the current transport through the material. In addition, silicon must be produced starting from its mineral compounds in the form of a pure block of material, then cut in wafer substrates on which lithographed mask is applied. Finally the wafer is chemically managed to take away the non-impressed material. The process is long and highly specialized. Very complex software packages must be used to design details of chips and the final production cost is non-negligible.

On the other hand, 100 nm is at the border of nanotechnology. That means the need is to control matter at the molecular–atomic level during the fabrication of devices or materials within this size range. With nanotechnology, the building process inverts the top–down process on which the use of silicon compounds is based. Macro structures can be built by chemically assembling individual molecules or by stimulating the self-assembling properties of organic materials. In this way, dimensions of structures can be sub-micrometric and as large as desired: it is sufficient to stop the growth process as the structure reaches the desired dimensions.

The birth of nanoscience is commonly attributed to Richard Feynman, the physicist who in a famous speech given at the American Physical Society meeting at Caltech on December 29, 1959 claimed: "*The future is in the smaller things*". He introduced the concept of nanotechnology as the controlled manipulation of matter at the nanometer length scale suggesting that "*There's a plenty of room at the bottom*". Since then, thousands of physicists applied to nanoscience. New materials have been created and the new physics phenomena observed in the nanoscale opened a new scenario on the future of science and technology.

2. Carbon nanotubes

Since 15 years, a new material has been continuously increasing its importance: carbon in the form of nanotubes. Carbon is present in nature in several allotropic forms. The most well-known are graphite and diamond. In 1985, the discovery of fullerene opened a new scenario: carbon can be assembled in the nanoscale as tiny droplets of graphene. The C_{60} structures, 7.1 Å radius, were produced by arc discharge [2]. Six years later, graphene sheets rolled up as tubes with nanometer diameter, tens of micron long, were produced with similar chemical process first as multiwalled carbon nanotubes (MWCNT) [3], then as single wall carbon nanotubes (SWCNT) [4]. Their structure's properties are fully determined by the chiral indexes of rolling process [5]. From those, CNT diameter is fixed, as well as electrical properties, i.e. they will be metallic or semimetallic or semiconductors according to the chiral indexes.

Depending on the specific interests, and targeted applications, nanotubes are regarded as either single molecules or quasi-one-dimensional crystals with translational periodicity along the tube axis. As there are an infinite number of ways of rolling a sheet into a cylinder, the large variety of possible helical geometries defining the tube chirality provides a family of nanotubes with different diameters and microscopic structures. This dependence on the atomic configuration is quite unique in solid-state physics.

Applications of carbon nanotubes range from reinforcement of composites or conductive plastics to electrodes for batteries or flat screens, field effect transistors, chemical or force sensors and electromechanical memory. These applications have been demonstrated in bulk as well as on surfaces and on individual tubes.

A very large literature has been published on the properties of CNTs. Their very peculiar properties have been intensively investigated everywhere in the world and thousands of researchers produce, study and manipulate CNTs in a number of Research Laboratories. Most of them are convinced that the Post Silicon ERA has turned into the carbon ERA.

From the point of view of photodetection, semiconducting nanotubes show interesting optoelectronic properties in the region of near-to-mid infrared (from ~1 to ~15 μm) tied to their electronic characteristics. Due to their quasi-1D structure, SWCNTS feature quasi-discrete energy levels rule by van Hove singularities in the density of states. The energy gap is a function of the diameter, as approximately given by the relationship: $E_{gap} = a/d$, where $a = 0.0284\,eV\,nm$ and d is the diameter in nm. This implies that for the SWCNT, with diameter from about 1 to 2 nm, the fundamental gap (eh_{11}) varies from 0.4 to 0.7 eV, corresponding to a wavelength range from 1.5 to 3 μm [6]. A layer of multiwall carbon nanotubes covers instead a wide range of diameters and chiralities whose characteristics have not yet been fully understood, offering a device sensitive to a wide range of wavelength frequencies, from 200 nm up to several microns.

The capability of CNTs to detect radiation has been demonstrated by various authors [7,8] who measured a variation in the nanotube's conductivity when illuminated with IR radiation. The pioneering work of Xu [7] suggested the possibility of realizing uncooled bolometers for space physics made of CNT. Photoconductivity of individual, ropes and films of CNTs has been also investigated in the visible [9] and IR [10] spectral regions. Photon induced charge carrier generation in single wall carbon nanotubes and subsequent charge separation across the metal–carbon nanotube contacts is believed to cause the photoconductivity variations [9]. Mesurements in the UV region, to the best of our knowledge, are still missing.

In this scenario, the Italian National Institute for Nuclear Physics (INFN) promoted the gruppo INFN per le nano tecnologie (GINT) collaboration with the aim to explore the CNT properties and their potential application to photodetection.

3. The GINT (gruppo INFN per le nanotecnologie) activity

The GINT collaboration was born in 2005 and has been funded by INFN on the base of an activity program three years long. The collaboration actually consists of 41 physicists from 6 Italian Universities and several other scientific institutions. Activities started in January 2006 with the aim to explore the possibility of using carbon nanotube-based devices to provide new

opportunities for obtaining large-area and highly sensitive radiation detectors.

The question has been addressed investigating the nanotubes' behaviour in different conditions with a number of different diagnostic methods. In the following, we summarize the main item and most significant results obtained.

3.1. Nanotubes production

The first aim was the development of an improved process to grow carbon nanotubes on various substrates with different geometry using chemical vapour deposition (CVD) [11]. Fig. 1 shows two types of nanotubes grown at different CVD temperatures. On the left side ($T = 500\,^{\circ}C$), the crystalline structure of nanotubes is not yet well developed and the tubes look like carbon nanofibers. On the right side ($T = 700\,^{\circ}C$), instead, a clear one-dimensional and crystalline structure is visible. CNTs are well aligned, with uniform density and uniform length of about 20 μm. The substrate is a $1 \times 1\,cm^2$ silicon, 500-μm-thick, and CNTs cover uniformly the entire surface.

TEM images carried out by high resolution transmission electron microscopy (HRTEM, JEOL JEM 2010) of both kinds of CNTs are reported in Fig. 2. Nanotubes grown at low temperature present an average length of 150 nm, a diameter of tens nanometers and a round edge of 20–30 nm. The structure is more similar to a filled cylinder than to a tube, with the external shell not well graphitized (Fig. 2a). Nickel particles used as catalyst appear to be encapsulated close to the apex of the structure (Fig. 2b).

At 700 °C temperature, the CVD process produces nanotubes of very different kinds. Their structure is well defined as a multiwall made in average of 10–15 tubes, with an inner diameter of 5–10 nm, an outer diameter ranging from 15 to 25 nm (Fig. 3a and b) and a length of tens of micron. Several tubes look bended. Inclusions of particles are also present (Fig. 3c). Most of them are uncapped (Fig. 3d).

3.2. Raman spectroscopy

Complementary structural investigations have been carried out by micro-Raman spectroscopy [12]. While HRTEM features unique imaging capabilities, Raman spectroscopy has the advantage of being a noninvasive technique suitable for in-situ, real-time analysis of carbon-based materials and devices [13–16].

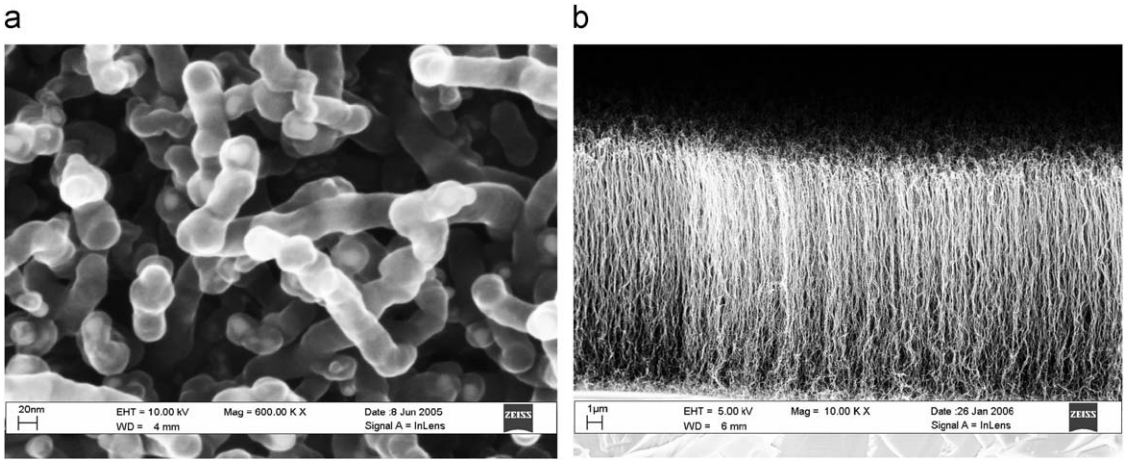

Fig. 1. Left: carbon nanotubes grown by CVD at a temperature of 500°; Right: CNT growth at 700°.

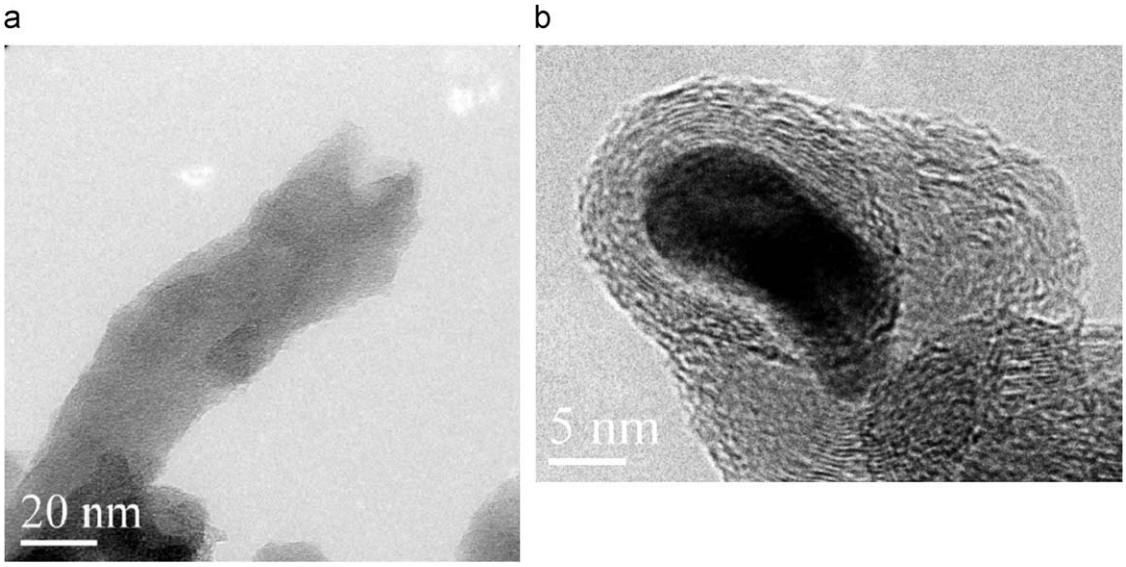

Fig. 2. (a) Structure of a 500 °C carbon nanotubes; (b) nickel catalyst particle encapsulated at the apex of the structure.

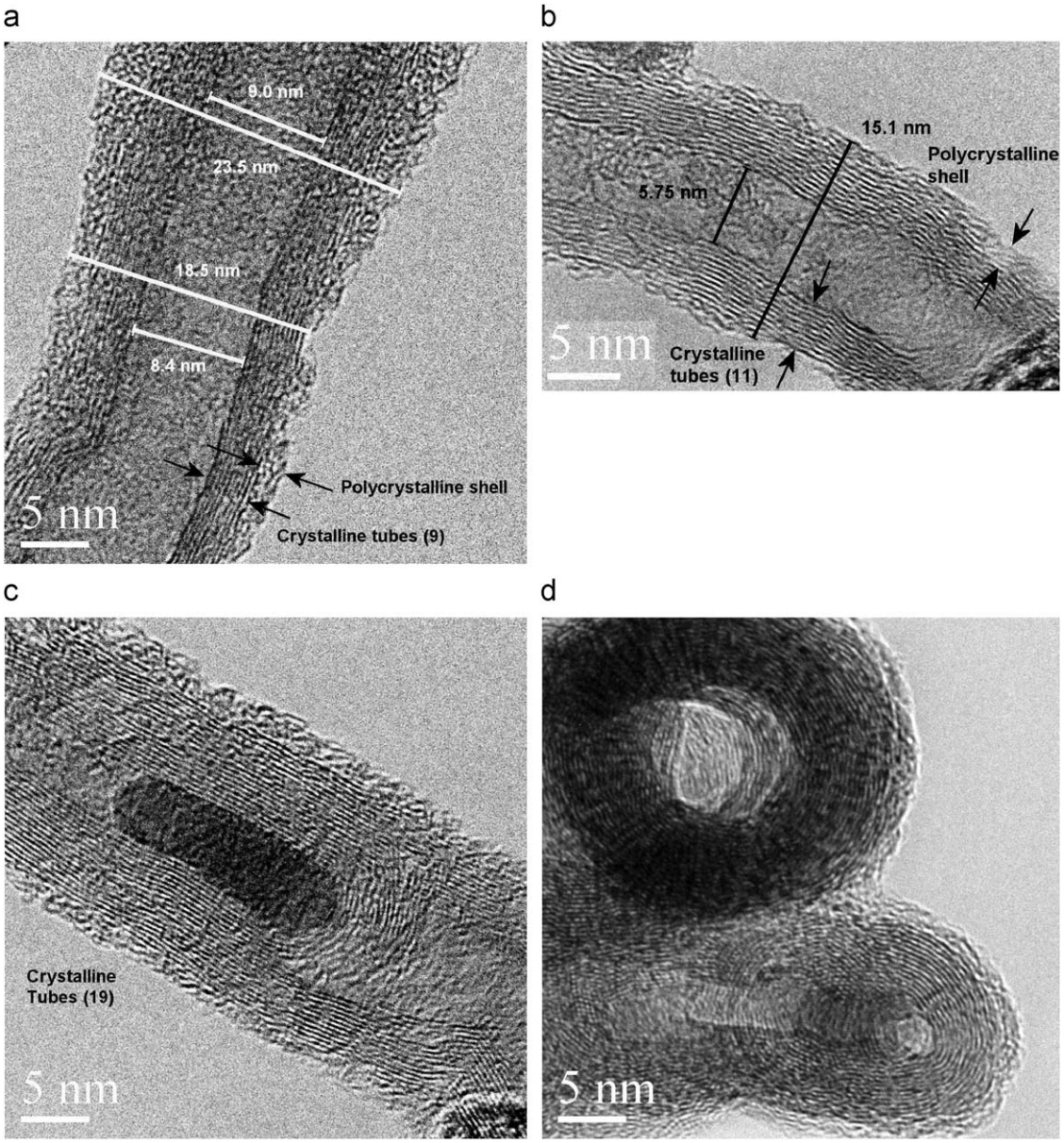

Fig. 3. TEM images of 700° of CNTs.

Typical Raman spectra of CNTs include three characteristic regions: the radial breathing modes (RBM—$50<\omega<400\,\mathrm{cm}^{-1}$) indicating the radial in-phase motion of C atoms; the disorder-induced band (D modes-$1200<\omega<1400\,\mathrm{cm}^{-1}$) due to structural defects and substitution impurities and G modes (HEM—$1450<\omega<1650\,\mathrm{cm}^{-1}$) measuring the breaking of symmetry of graphene due to tangential vibrations.

Fig. 4 (red line) shows the Raman spectrum of an MWCNT sample grown at 700 °C. We observe the D and the G bands (1300–1400 and 1530–1640 cm^{-1}, respectively) typical of carbon materials, together with the fingerprint of the silicon substrate (520 and 980 cm^{-1}). Compared to amorphous carbon nanofibers (Fig. 4, black line), the MWCNTs show a much narrower D band (full-width at half-maximum of 72 against 263 cm^{-1}), as well as a strong 2D mode at 2653 cm^{-1}. Both elements indicate a good degree of graphitization, but still there is a presence of a non-negligible amount of defective polycrystalline carbon sites.

3.3. Field emission of CNTs

Owing to their high aspect ratio, extremely small radius of curvature, unique electric properties, high chemical stability and mechanical strength, carbon nanotubes can be extraordinary field emitters and interest in their applicability for field emission (FE) devices has been steadily growing since their discovery.

FE occurs when electrons tunnel out a solid through the surface potential barrier whose width is reduced by the application of an external electric field. The emission current depends on the electric field at the emitter surface, E_S, and on the work-function, Φ, i.e. the effective surface-vacuum barrier height. The "elementary" Fowler–Nordheim (F–N) model, derived for a flat metallic surface at 0 K assuming a triangular potential barrier, predicts the following exponential behaviour of the emitted current:

$$I = aE_{\mathrm{eff}}^2 \exp(-b/E_{\mathrm{eff}})$$

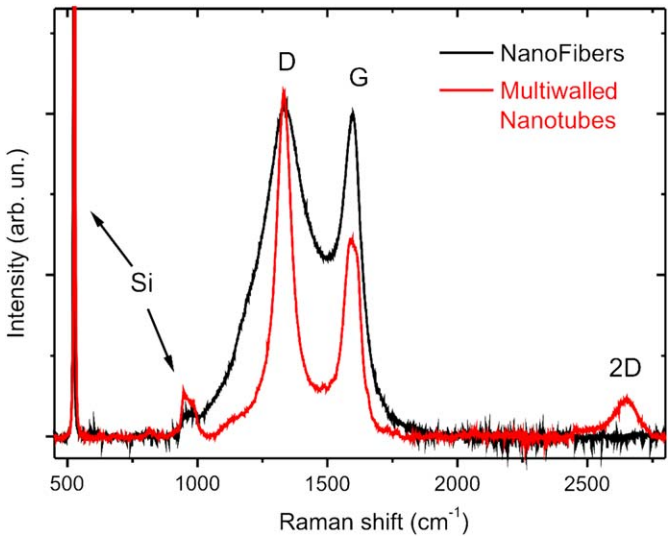

Fig. 4. Raman spectrum of MWCNTs (red line) compared to amorphous carbon nanofibers (black line).

where E_{eff} is the effective field at the emitter surface, and a and b are constants related to the geometry and to the workfunction. CNTs are very good emitters because the coefficient corresponds to the ratio h/r where h is the nanotube length ($>10\,\mu m$) and r is the nanotube radius ($\sim 10\,nm$). The maximum current from a single MWNT is 0.2 mA [17] For this reason, CNTs are used for new monitors and X-ray sources.

For the measurement of the FE current, we used the nanometric probe of a high vacuum omicron AFM/STM system as anode; the voltage was applied and the current was measured by means of a source-measurement unit (SMU) of a Keithley 4200-SCS. A detailed scheme of the apparatus is shown in Fig. 5a. The sharp metal-coated polysilicon probe (of conical shape, height$\sim$25 μm, aperture of 30° and curvature radius $r<35\,nm$) enables local FE measurements over a limited circular region (whose radius is less than 1 μm) containing at most few hundred CNTs. Furthermore, the sub-micrometric inter-electrode distance let achieve high electric fields (up to 250 V/μm) with a modest voltage source. Voltage sweeps were performed on the allowed voltage range up to +210 V and the current flowing through the tip was measured with an accuracy better that 1 pA. Measurement at high vacuum $\sim 10^{-8}$ mbar and at $d \approx 2\,\mu m$ is shown in Fig. 5b. After an electrical stress, consisting of a few voltage sweeps, necessary to stabilize the emission, a series of 5 sweeps is recorded. Some negligible sweep-to-sweep variations are found, while less-noisy curves are observed with respect to the analogous measurements performed at a lower vacuum [18].

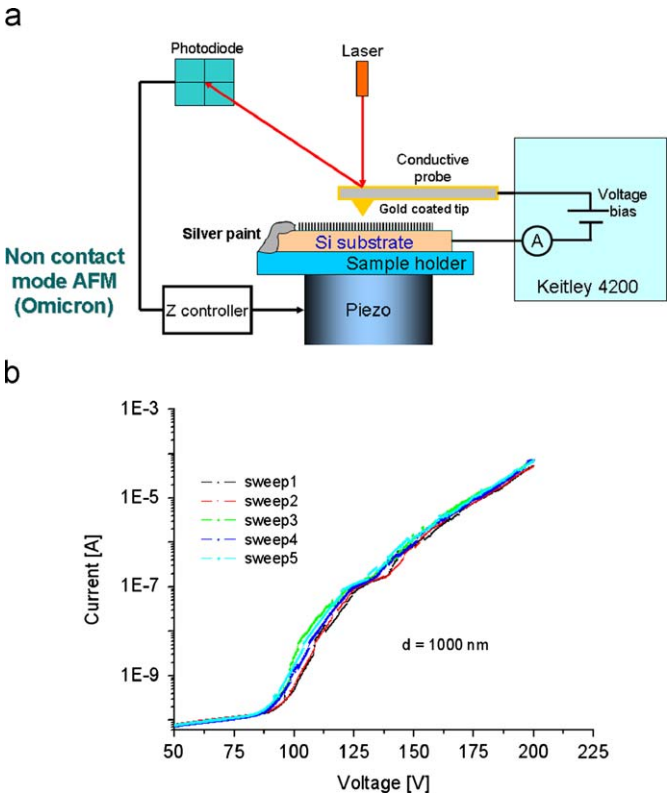

Fig. 5. (a) AFM probe used as counter-electrode (anode) for the measurement of the FE current from a vertically aligned array of MWCNTs. The whole apparatus consists of a vacuum chamber hosting an AFM/STM connected to an external source measurement unit; (b) Field emission current versus bias voltage in (b) logarithmic scale.

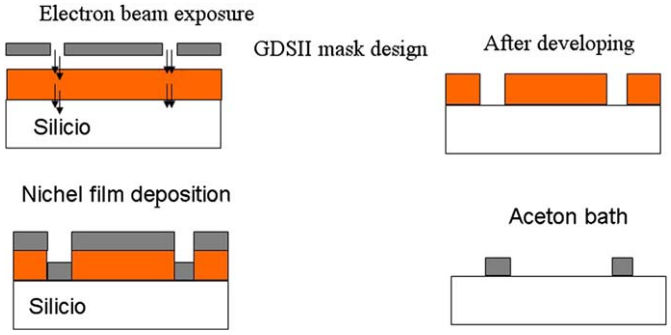

Fig. 6. The lift-off process used for CNT growth patternization.

3.4. Nanolithography and patternization

In order to grow the carbon nanotubes with a definite pattern, we have developed a procedure based on a lift-off process. "Lift-off" is a method for making metallic patterns on a substrate, especially for those noble-metal thin films such as platinum, tantalum, nickel or iron, which are difficult to be etched by conventional methods. The general lift-off process is as follows: first a pattern is defined on a substrate using photoresist. A film, usually metallic, is deposited all over the substrate, covering the photoresist and areas in which the photoresist has been cleared. During the actual lifting-off, the photoresist under the film is removed with a solvent, taking the film with it, and leaving only the film that was deposited directly on the substrate. In this way the assisting material layer is exposed (Fig. 6a). This layer is then wet-etched so as to undercut the resist (Fig. 6b). The metal is subsequently deposited on the wafer, by a thermal evaporation process (Fig. 6c). The resist is removed taking away the unwanted metal with it. The assisting layer is then stripped off too, leaving the metal pattern alone (Fig. 6d). The dimension of our pattern spreads from 10 μm down to 100 nm. This is obtained with an Electron Beam Lithography system.

Fig. 7 reports some results obtained with the combined use of nanolithography and lift-off process. A square matrix of 10×10 pixels, $4 \times 4\,\mu m^2$ each, is shown in Fig. 7a; pixels are made of a dense layer of nanotubes, as shown in Fig. 7b, and can assume the desired form, for example the INFN logo shown in Fig. 7c. What is important is that nanotubes grow only where the lift-off process left the catalyst: no carbon compounds appear to be present outside the pixel, as shown in Fig. 7c.

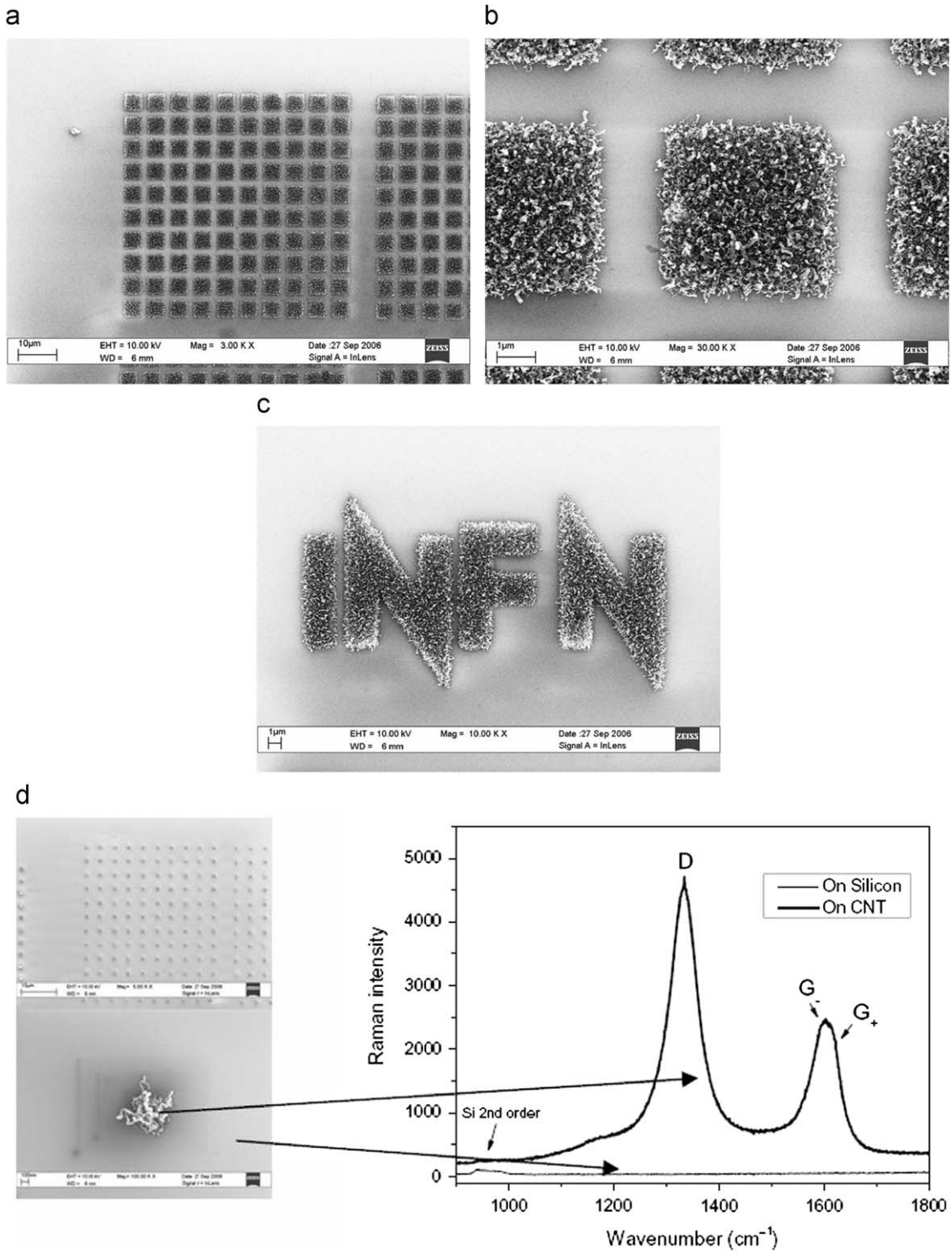

Fig. 7. (a) A square CNT matrix of 10×10 pixels,$4 \times 4\,mm^2$ obtained with a lift-off process on lithographed mask; (b) individual $2 \times 2\,\mu m^2$ CNT pixel; (c) the INFN logo made of CNT in micrometric scale; (d) Raman image of CNT and silicon substrate.

3.5. Sensitivity to the radiation

In order to investigate the sensitivity of carbon nanotubes to the radiation, MWCNTs have been grown by CVD at a temperature of 750 °C on a sapphire substrate as shown in Fig. 8a (black area in the centre). Two electrodes have been obtained by platinum deposition on the CNT layer. Fig. 8b shows the transmittance curve for two different samples obtained by means of a commercial UV/NIR Spectrometer. The sapphire transmittance curve is also reported. The different behaviour is due to the different CNT density. In Fig. 8c, the absorbance curve indicates a strong adsorption peak at around 5 eV, which is close to the π plasmon frequency in carbon materials such as graphite, C60 and SWNTs [19].

The photosensitivity of CNTs has been investigated also measuring the photocurrent collected at the two electrodes obtained illuminating the samples with monochromatic radiation in the UV–VIS–NIR range. Photocurrent normalized to the number

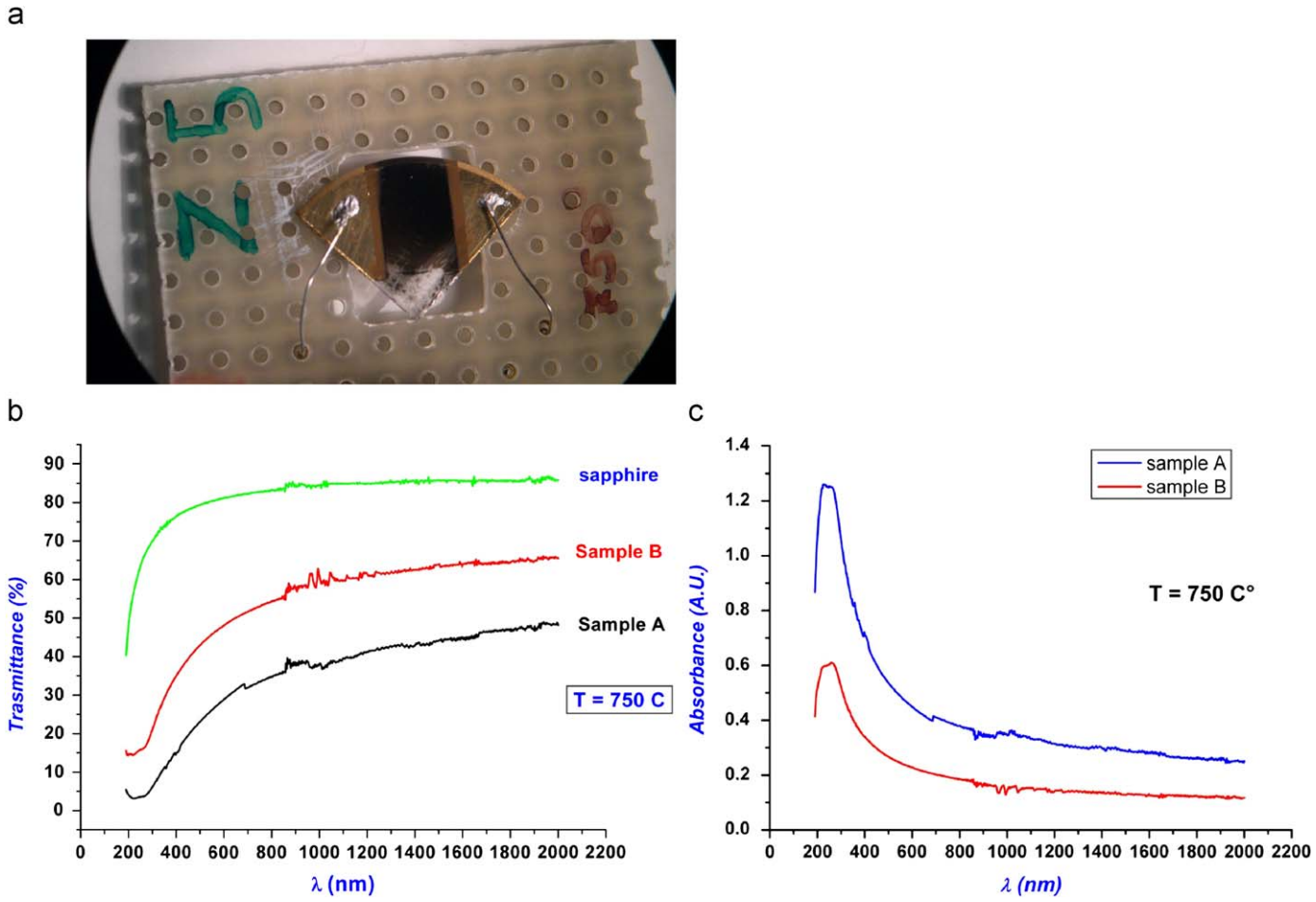

Fig. 8. (a) Image of the sample used to measure the MWCNT responsivity; (b) transmittance curve of two samples; (c) the absorbance curve of samples.

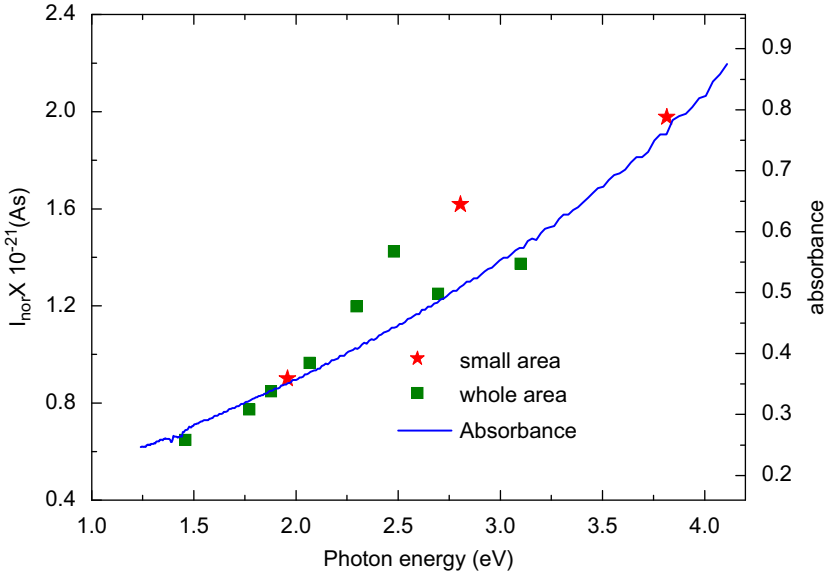

Fig. 9. Photocurrent normalized to the number of photons I_{nor} vs. photon energy, obtained illuminating the whole surface of an MWCNT sample with filtered light (■) as well as small part of the surface with laser spots (ξ). Continuous line indicates the absorbance spectrum of the same MWCNT sample.

of photons I_{nor} vs photon energy, at a polarization voltage $V_{pol} = 160$ V, obtained illuminating the whole surface of an MWCNT sample with filtered light (■) as well as small part of the surface with laser spots (ξ) of 1.96, 2.81 and 3.82 eV as shown in Fig. 9. Continuous line indicates the absorbance spectrum A of the same MWCNT sample. I_{nor} increases with increasing the photon energy from the ultraviolet towards the near-infrared region according to the results reported by others [20] in the

1.5–3.8 eV range. It is worth observing that the measurements performed by laser irradiation of a small part of the sample surface far from the Au contacts show that the photocurrent is produced only by the MWCNTs. The photocurrent values have been multiplied by a scaling factor that takes into account V_{pol} and the illuminated area.

3.6. Sensitivity to pulsed light: a CNT detector prototype [21]

The CNT detector layout is shown in Fig. 10. MWCNTs have been grown by chemical vapour deposition (CVD) on a sapphire substrate in the 100 μm space between two comb-like electrodes made of gold and platinum, 250-nm-thick, 100-μm-large. The detector prototype is 4 mm large, 6 mm long, 0.5 mm thick. The inert sapphire substrate prevents the contribution of other materials to the photoresponsivity of MWCNTs and permits the study of the behaviour of the pure nanotube layer. On the left of Fig. 10, the structure of the electrodes is shown. In between the platinum electrodes, the CNT black layer is clearly visible. Nanotubes have been grown using nickel nanospheres as catalyst deposited on a silicon nitrate layer, 30-nm-thick, and submitted to the CVD process at a temperature of 500 °C. The resulting nanostructures obtained are shown in the right of the figure.

An Nd–Yag laser beam, >10 ns pulse duration, 10 Hz repetition rate at three different wavelengths, 1064, 532 and 355 nm (respectively fundamental, second and third harmonic of the neodymium laser), is addressesd on the detector and a voltage ranging between −25 and +25 V is applied to the electrodes. These signals can then be easily observed by means of an oscilloscope closed on its load resistance of 50 Ω without any further amplification, as shown in the bottom of Fig. 10. By integrating the signals acquired using the oscilloscope over the monitored time window, the charge generated in the photoconversion process can be easily measured.

Fig. 11 shows signals detected at various laser wavelenghts and different laser intensities. For each plot, a, b and c signals at various values of drain voltage are compared. It can be seen that in all cases, signal peak value as well as the signal charge increases with the voltage value in a linear relation. This suggests that the detector is not collecting the full charge generated in the photoconversion process, but it runs with a very low efficiency. On the other hand, we cannot increase the value of the drain voltage because of the considerable dark current value shown in Fig. 11d: nanotubes appear to be a quasi metallic compound with an ohmic resistance of 2.18 kΩ.

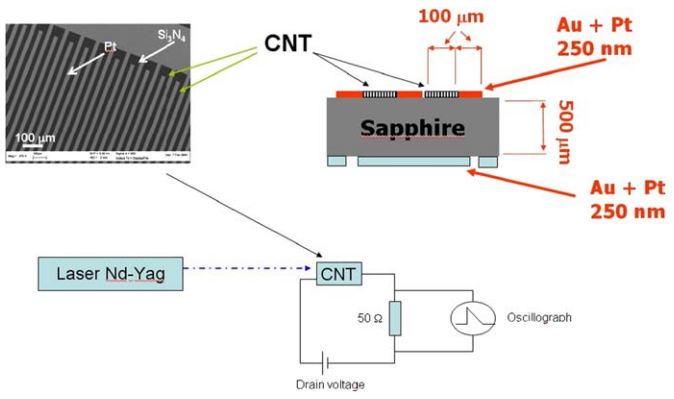

Fig. 10. (Top) layout of CNT detector; (bottom) experimental setup.

The plot of Fig. 12a shows the comparison between signals at different wavelenghts drained with 25 V voltage and normalized at the same laser power. It appears evident that signals generated with UV radiation is much more intense than those induced by IR or visible light. The measured conversion efficiency, defined as the ratio between the number of electrons collected at electrodes and the number of incident photons, without taking into account reflections, geometrical factors, etc., is plotted in logarithmic scale in Fig. 12b. This plot enhances the strong difference in the photoconversion efficiency between UV and IR regions.

It must be noted that the CNT photoconversion efficiency in the near IR (1064 nm) is only 2% of the conversion efficiency at 355 nm. This confirms independent measurements obtained with a similar larger area device analized with a UV/NIR spectrometer and reported in Fig. 8c.

3.7. Model simulation—electron affinity and ionization potential of carbon nanotubes

The electronic properties of single wall carbon nanotubes with methods rooted from the density functional theory have been investigated [22]. We have analyzed two classes of systems: the isolated nanotube and the corresponding periodic array. We report the dependence of EA and IP on either the nanotube length (for the isolated nanotube) or the lattice parameter (in the case of the array).

The calculations have been performed using two different computational schemes. The first one is an all-electron method as implemented into the DMol^3 package (Accelrys Inc.). The second one is based on a pseudopotential plane-wave method as implemented in the QUANTUM-ESPRESSO code. All calculations have been done using the generalized gradient approximation (GGA) with the Perdew, Burke and Ernzerhof (PBE) correlation functional.

Our calculations have been focused on armchair (5,5) nanotubes of different lengths, whose edges have been passivated with hydrogen atoms. The electron affinity is defined as $EA = E(N)-E(N+1)$ where $E(N)$ and $E(N+1)$ are the total ground-state energies in the neutral (N) and single charged ($N+1$) configurations. The ionization potential is as well defined as $IP = E(N-1)-E(N)$. Once the EA and IP have been calculated, an important physical variable giving information on the nanotube reactivity is the Mulliken electronegativity, which is defined as $\chi = (EA+IP)/2$. An interesting aspect of this definition is that it is identical to the work function of a periodic nanotube assuming, for the case of a semiconducting tube, a Fermi level sitting at midgap.

We start the discussion by showing the numerical results on the work function (WF). The periodic (5,5) nanotube is a zero-gap metal for which we obtain an all-electron WF of 4.37 eV. The plane wave calculation gives 4.28 eV. In a finite nanotube, quantum confinement may induce a strong dependence of the electronic properties on the nanotube length. To give a clear insight on this effect, we have calculated the EA and IP for a number of tubes with increasing length. The results are shown in Fig. 13 for an isolated nanotube.

The first observation to be made on this figure is that both EA and IP, as well as the gap, exhibit a regular oscillation on increasing the nanotube length, in agreement with previous band-gap calculations. The quantum confinement effect is evidenced by the fact that EA and IP tend, for long nanotubes, to approach each other. An even more interesting aspect of the results shown in Fig. 13 is that electronegativity is not influenced by these strong oscillations and it is nearly independent of nanotube length. Indeed, χ has an overall variation of about 0.5–0.6 eV.

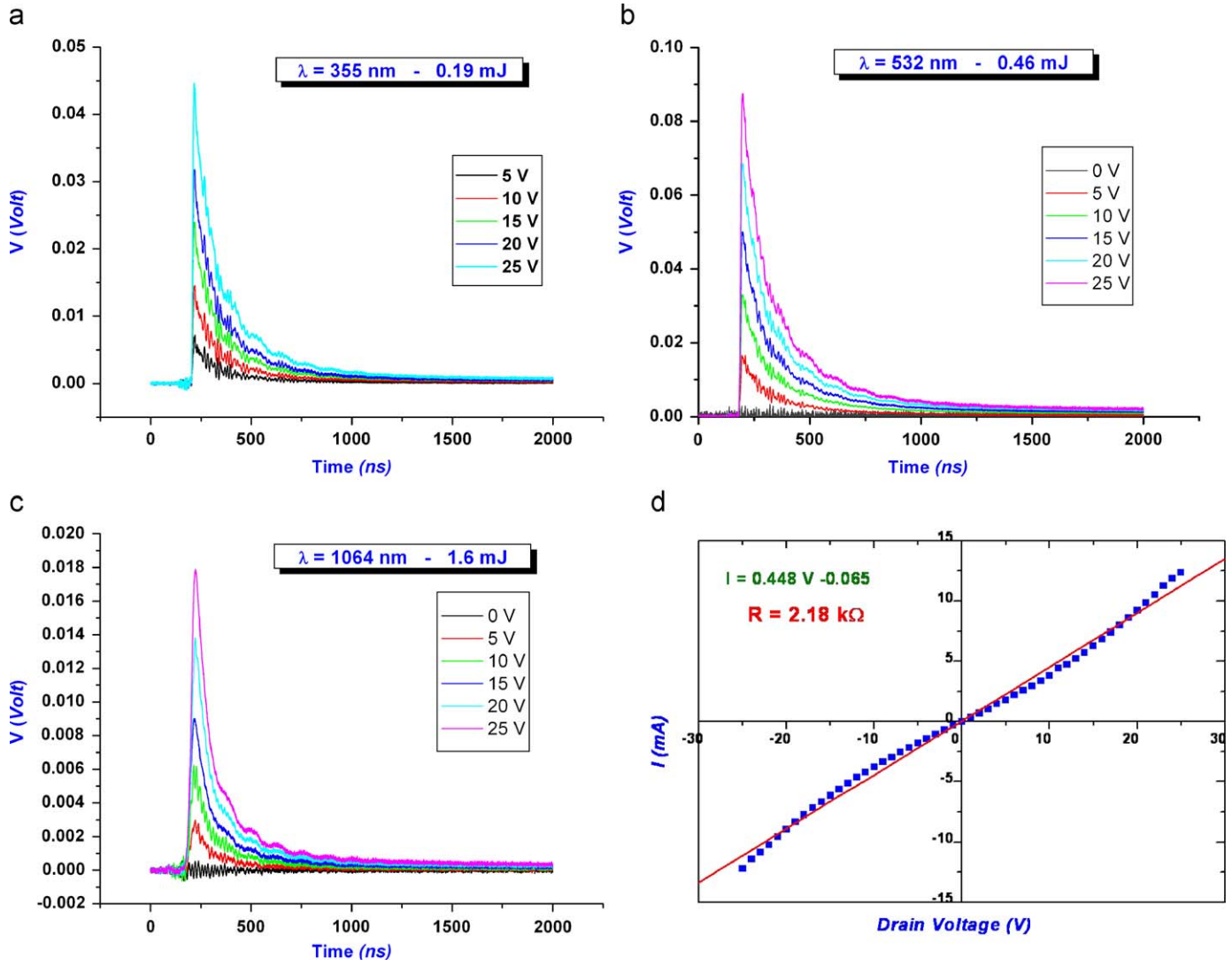

Fig. 11. Signals detected at various laser wavelengths and different laser intensities.

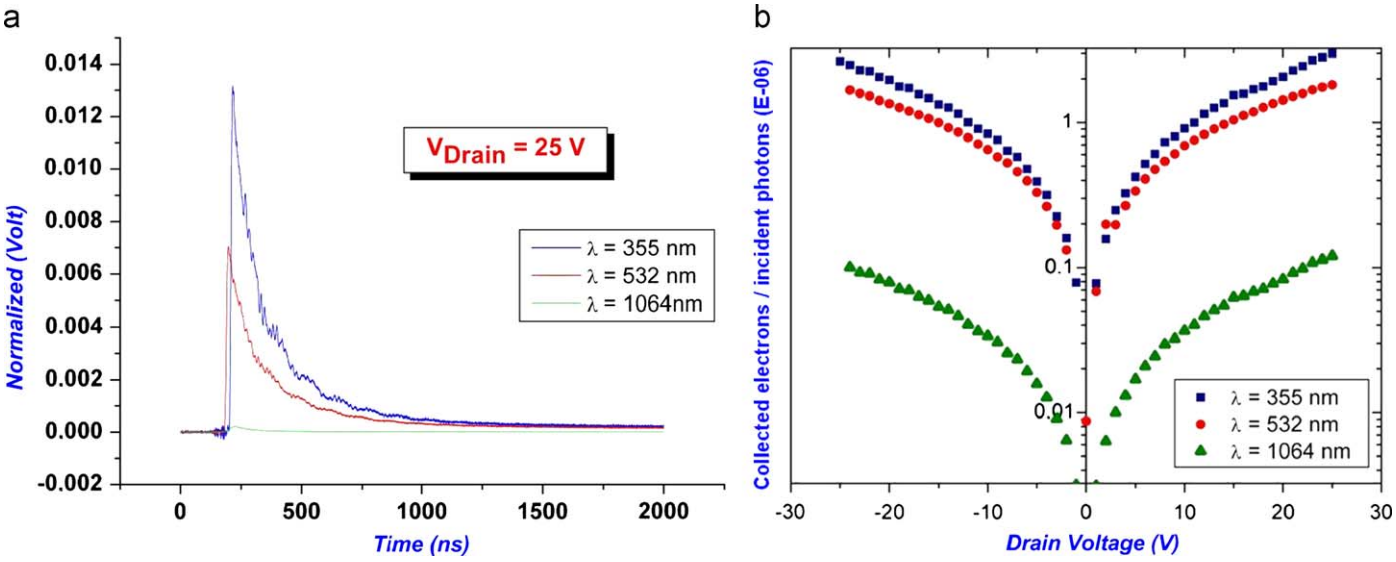

Fig. 12. (a) Comparison between signals at different wavelenghts drained with a 25 V voltage and normalized at the same laser power; (b) The measured conversion efficiency, defined as the ratio between the number of electrons collected at electrodes and the number of incident photons.

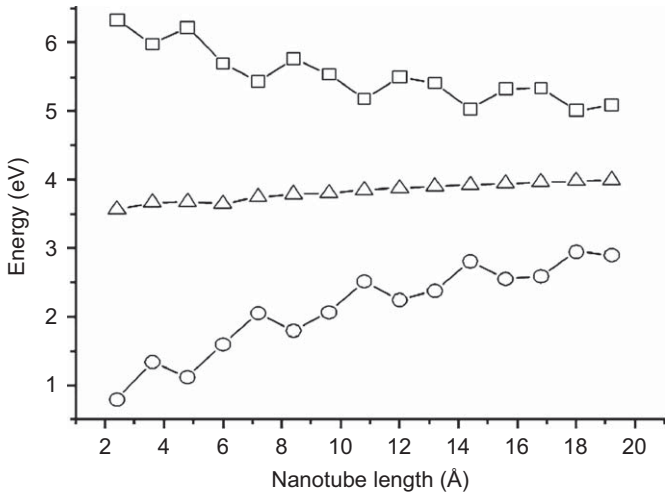

Fig. 13. Ionization potential (squares), electron affinity (circles) and electronegativity (triangles) of an H-pass (5,5) nanotube as a function of its length.

4. Conclusion

The modern silicon technology is actually at the border of nanotechnology and quantum effects begin to assume a strong relevance in the new generation of very high integration scale. The most recent gate developed by Intel is only 45 nm and is perfectly on the line of Moore's law declaiming that the number of transistors in a chip doubles every two years. At higher densities it must be foreseen strong limits due to the heat generated by electrons crossing internal junctions and electrodes. At the moment, the most recent silicon radiation detector is the Silicon Photo Multiplier, a matrix of $40 \times 40\,\mu m^2$ pixels grouped in mm^2 area, single photon sensitive in the visible wavelength range.

With silicon technology, the final product is obtained by means of the so-called "top-down" process: starting from macroscopic material, the matter is manipulated in such a way to obtain many microscopic elements. This process is very critical and expensive, and the final product is a result of a long and sophisticated process. Nanotechnology instead is based on a reverse approach: nano and micromaterials are built by grouping individual atoms and molecules, in a so-called "bottom-up" process. The final object dimensions depend on the duration of building process. This new approach is very cheap and relatively easy to do, being mostly a chemical process. This opens a door to the future, allowing the extension of Moore's law in the nanoscale world.

Among the new nanostructured materials, carbon nanotubes appear to be the most promising because of their unique physical and electrical properties. It has been demonstrated that they are characterized by an enhanced sensitivity to the radiation on a wide wavelength range, particularly important in the UV region. This opens the possibility to use this new material to build large-area photocathodes sensitive in the fluorescence-Cherenkov light-emission region (300–400 nm). In addition, they can be grown on a surface according to a finely pixelled mask obtained by means of nanolithography processes. Commonly, people refer to them claiming to be at the beginning of the post-silicon era.

The GINT experiment investigated successfully the property of carbon nanotubes concerning photodetection. The first photodetector made of carbon nanotubes has been built and characterized. The measured photocurrent increases towards the UV wavelength region in accordance with the absorbance increase of CNTs in this interval.

Acknowledgments

We acknowledge the CNR—Istituto per la Microelettronica e Microsistemi, Sez. di Catania for the TEM measurements. F. Bonaccorso, B. Fazio and C. Vasi are acknowledged for fruitful discussions.

We also are grateful to Prof. Eugenio Nappi for his precious suggestions and stimulating discussions.

References

[1] B. Dolgoshein, et al., Nucl. Instr. and Meth. A 504 (2003) 48.
[2] H.W. Kroto, R.F. Curl, R.E. Smalley, Rice University, 1985.
[3] S. Iijima, Nature, 354, NEC Laboratories, 1991 (p. 56).
[4] S. Iijima, E.T. Ichihashi, Nature 363 (1993) 603.
[5] S. Reich, C. Thomsen, J. Maultzsch, Carbon Nanotubes: Basic Concepts and Physical Properties, Wiley-VCH, 2003.
[6] R. Saito, G. Dresselhaus, M.S. Dresselhaus, Physical Properties of Carbon Nanotubes, Imperial College Press, 2003.
[7] I.M. Xu, Infrared Phys. Technol. 42 (2001) 485.
[8] M.E. Itkis, Science 312 (2006) 413.
[9] Shaoxin Lu, et al., Nanotechnology 17 (2006) 1843.
[10] I.A. Levitsky, W.B. Euler, Appl. Phys. Lett. 83 (9) (2003) 1857.
[11] Dobkin, Zuraw, Principles of Chemical Vapor Deposition, Kluwer, 2003.
[12] A. Jorio, M.A. Pimenta, A.G. Souza Filho, R. Saito, G. Dresselhaus, M.S. Dresselhaus, New J. Phys. 5 (2003) 138.
[13] A. Hartschuh, et al., Phys. Rev. Lett. 90 (2003) 095503.
[14] F. Wang, W. Liu, Y. Wu, M.Y. Sfeir, L. Huang, J. Hone, S. O'Brien, L.E. Brus, T.F. Heinz, Y. Ron Shen, Phys. Rev. Lett. 98 (2008) 047402.
[15] J. Maultzsch, H. telg, S. Reich, C. Thomsen, Phys. Rev. B 72 (2005) 205438.
[16] F. Bonaccorso, C. Bongiorno, B. Fazio, P.G. Gucciardi, O.M. Marago, A. Morone, C. Spinella, Appl. Surf. Sci. 254 (2007) 1260.
[17] M.S. Dresselhaus, G. Dresselhaus, P.h. Avouris, Carbon Nanotubes: Synthesis, Structure, Properties and Applications, Springer, Berlin, 2001.
[18] A. Di Bartolomeo, A. Scarfato, F. Giubileo, F. Bobba, M. Biasiucci, A.M. Cucolo, M. Passacantando, S. Santucci, Carbon 45 (2007) 2957.
[19] M. Knupfer, T. Pichler, M.S. Golden, J. Fink, A. Rinzler, R.E. Smalley, Carbon 37 (1999) 733.
[20] P. Castrucci, F. Tombolini, M. Scarselli, E. Speiser, S. Del Gobbo, W. Richter, M. De Crescenzi, M. Diociaiuti, E. Gatto, M. Venanzi, Appl. Phys. Lett. 89 (2006) 2531.
[21] A. Ambrosio, et al., Nucl. Instr. and Meth. Phys. Res. A 589 (2008) 398.
[22] F. Buonocore, et al., Nanotechnology 19 (2008) 025711.